SCIENCE CHINA
Earth Sciences

• RESEARCH PAPER •

June 2016 Vol.59 No.6: 1308–1316
doi: 10.1007/s11430-015-5251-y

Effects of tide-surge interactions on storm surges along the coast of the Bohai Sea, Yellow Sea, and East China Sea

XU JunLi[1], ZHANG YuHong[2], CAO AnZhou[1], LIU Qiang[2*] & LV XianQing[1]

[1] *Key Laboratory of Physical Oceanography (Ocean University of China), Ministry of Education, Ocean University of China, Qingdao 266100, China;*
[2] *College of Engineering, Ocean University of China, Qingdao 266100, China*

Received August 27, 2015; accepted November 17, 2015; published online January 4, 2016

Abstract A two-dimensional coupled tide-surge model was used to investigate the effects of tide-surge interactions on storm surges along the coast of the Bohai Sea, Yellow Sea, and East China Sea. In order to estimate the impacts of tide-surge interactions on storm surge elevations, Typhoon 7203 was assumed to arrive at 12 different times, with all other conditions remaining constant. This allowed simulation of tide and total water levels for 12 separate cases. Numerical simulation results for Yingkou, Huludao, Shijiusuo, and Lianyungang tidal stations were analyzed. Model results showed wide variations in storm surge elevations across the 12 cases. The largest difference between 12 extreme storm surge elevation values was of up to 58 cm and occurred at Yingkou tidal station. The results indicate that the effects of tide-surge interactions on storm surge elevations are very significant. It is therefore essential that these are taken into account when predicting storm surge elevations.

Keywords Storm surges, Astronomical tides, Tide-surge interactions, Typhoon 7203, Coupled tide-surge model

Citation: Xu J L, Zhang Y H, Cao A Z, Liu Q, Lv X Q. 2016. Effects of tide-surge interactions on storm surges along the coast of the Bohai Sea, Yellow Sea, and East China Sea. Science China Earth Sciences, 59: 1308−1316, doi: 10.1007/s11430-015-5251-y

1. Introduction

People in coastal areas can be affected by storm surges, with these being abnormal increases or decreases in sea level induced by typhoons and atmospheric pressure disturbances (You and Seo, 2009; Yang et al., 2014). Storm surges can be positive or negative. A positive storm surge can result in significant loss of life and property damage, for example through the destruction of coastal infrastructure (Lin et al., 2012; Olbert et al., 2013; Haigh et al., 2014). Negative surges (Pousa et al., 2013) mainly jeopardise maritime safety and coastal engineering structures. It is vitally important to study storm surges along the coast, as results can provide useful information for risk-based flood management and engineering planning (Olbert et al., 2013).

Typhoons can bring about significant storm surges in coastal regions (Zhang et al., 2015; Yang et al., 2015), such as storm surges. To improve coastal storm surge forecasting, Peng et al. (2006) constructed a four-dimensional variational data assimilation algorithm using a tangent linear model and an adjoint model of the Princeton Ocean Model (POM). Peng et al. (2007) and Li et al. (2013) used this adjoint optimal technique to adjust initial conditions, boundary conditions, and the wind stress drag coefficient in the POM. Yin et al. (2009) simulated five typhoon storm surges in the East China Sea using a coupled model and suggested that a storm surge-wave coupled model should be used for storm surge prediction.

Storm surges can be aggravated if coinciding with a high spring tide or with a low neap tide (Maspataud et al., 2013; Olbert et al., 2013). In recent years, researchers have ex-

*Corresponding author (email: liuqiang@ouc.edu.cn)

plored the interactions between storm surges and astronomical tides in certain coastal areas using different methods. Zhang et al. (2007) utilised the two-way nested coupled tide-surge model to study the combined effects of storm surges and astronomical tides in the Taiwan Strait. Simulation results indicated that the influence of astronomical tides on storm surges should be taken into account in prediction models. Park et al. (2012) analysed the effects of water depth and astronomical tides on storm surges using the coupled numerical model PBL-ADCIRC. Results confirmed that the coupling of storm surges and tides is an essential consideration in coastal areas with shallow water depth and large tides. Antony et al. (2013) examined the dependency of surge maxima on tide magnitudes and phases, quantifying their interaction along the east coast of India and the head of the Bay of Bengal. They found that the strength of interaction tended to increase northward when tidal ranges and surge heights increased. Kong (2014) calculated and analysed 57 cases of Typhoon 7203 to study the impact of tidal waves on storm surges in the north of Liaodong Bay, using DHI Mike21.

However, little attention has been paid to the impacts of tide-surge interactions on storm surges along the coasts of the Bohai Sea, Yellow Sea, and East China Sea, all of which are vulnerable to such phenomena. In the present paper, we investigate the effects of tide-surge interactions on storm surge elevations during Typhoon 7203 using a two-dimensional coupled tide-surge model. Eight principal constituents (M2, S2, K1, O1, N2, K2, P1, and Q1) were introduced into the numerical model through open boundary conditions and tidal potentials. Meteorological driving forces that generate storm surges were provided by the wind forcing module and pressure field.

2. Coupled tide-surge model

The coupled tide-surge model is based on a depth-averaged two-dimensional flow model. This section describes the model framework in detail.

2.1 Basic equations

The governing equations used in the two-dimensional flow model are composed of depth-averaged equations of continuity and momentum.

$$\frac{\partial \zeta}{\partial t}+\frac{1}{a}\frac{\partial\left[(h+\zeta)u\right]}{\partial \lambda}+\frac{1}{a}\frac{\partial\left[(h+\zeta)v\cos\varphi\right]}{\partial \varphi}=0, \quad (1)$$

$$\frac{\partial u}{\partial t}+\frac{u}{a}\frac{\partial u}{\partial \lambda}+\frac{v}{R}\frac{\partial u}{\partial \varphi}-\frac{uv\tan\varphi}{R}-fv+\frac{ku\sqrt{u^2+v^2}}{h+\zeta}-A\Delta u$$
$$+\frac{g}{a}\frac{\partial\left(\zeta-\bar{\zeta}\right)}{\partial \lambda}+\frac{1}{\rho_w a}\frac{\partial P_a}{\partial \lambda}-\frac{\rho_a}{\rho_w}\frac{C_d W_x\sqrt{W_x^2+W_y^2}}{h+\zeta}=0, \quad (2)$$

$$\frac{\partial v}{\partial t}+\frac{u}{a}\frac{\partial v}{\partial \lambda}+\frac{v}{R}\frac{\partial v}{\partial \varphi}+\frac{u^2\tan\varphi}{R}+fu+\frac{kv\sqrt{u^2+v^2}}{h+\zeta}-A\Delta v$$
$$+\frac{g}{R}\frac{\partial\left(\zeta-\bar{\zeta}\right)}{\partial \varphi}+\frac{1}{\rho_w R}\frac{\partial P_a}{\partial \varphi}-\frac{\rho_a}{\rho_w}\frac{C_d W_y\sqrt{W_x^2+W_y^2}}{h+\zeta}=0, \quad (3)$$

where t is time; λ and ϕ are east longitude and north latitude, respectively; h is depth of undisturbed water; ζ is sea surface elevation, relative to the undisturbed level; $h+\zeta$ is total water depth; u and v are the east and north components of the current, respectively; $\bar{\zeta}$ is the adjusted height of equilibrium tides; R is the radius of the earth and $a=R\cos\phi$; $f=2\Omega\sin\phi$ is the Coriolis parameter (here, Ω is the angular speed of the Earth's rotation); k is the bottom friction coefficient; A is the horizontal eddy viscosity coefficient; Δ is the Laplace operator and $\Delta(u,v)=a^{-1}\left[a^{-1}\partial_\lambda\left(\partial_\lambda(u,v)\right)+R^{-1}\partial_\varphi\left(\cos\varphi\partial_\varphi(u,v)\right)\right]$; g is gravitational acceleration; P_a is atmospheric pressure on the sea surface; ρ_w=1025 kg m^{-3} is seawater density; ρ_a=1.27 kg m^{-3} is air density, and W_x and W_y are the x and y components of the surface wind field. In this paper, the wind-stress coefficient C_d was calculated on the basis of wind velocity U_{10} measured at 10 m above mean sea surface (Wu, 1982):

$$C_d=\left(0.8+0.065\times U_{10}\right)\times 10^{-3}. \quad (4)$$

2.2 Initial conditions and boundary conditions

In the present coupled model, initial values of current velocity and surface elevation were calculated using the tidal model. Along closed boundaries, it was assumed that no water would be allowed to flow to the coast; that is, the normal component of the current would be zero. This can be expressed as $\vec{u}\cdot\vec{n}=0$, where $\vec{u}=(u,v)$ is the current vector and $\vec{n}$ is the outward unit vector.

The main areas of research for this study were the Bohai Sea and northern Yellow Sea. Suppose that there is a current with a speed of 0.5 m s^{-1} at the open boundary point (130.9°E, 33.8°N). It will take 24 days for the current to arrive at the LianYunGang tidal station (119.45°E, 34.75°N). However, the simulation time of the typhoon is only three days. In this case, the open boundary conditions of the storm surge are negligible. The present open boundary conditions are therefore determined as sea-surface elevations caused by tides, as follows:

$$\zeta=\sum_{j=1}^{J} f_j H_j\cos\left(\omega_j t+u_j+v_j-g_j\right), \quad (5)$$

where H_j and g_j are the amplitude and phase-lag of the jth tidal constituent, respectively; ω_j is angular speed; v_j is the initial phase angle; f_j is the nodal factor; and u_j is the

nodal angle.

2.3 Wind forcing module

Meteorological driving forces that generate storm surges are mainly composed of surface wind stress and pressure gradient forces (Zhang et al., 2007; Chen et al., 2012). It is therefore critical for tropical storm simulations to determine surface wind and pressure fields.

Compared with the impact of a pure tropical storm, that of the background wind field on a storm surge is probably weaker; however, it should not be neglected (Wen et al., 2008; Tang et al., 2013). According to Wen et al. (2008), the synthetic wind field is given by reanalysis surface winds data of the National Centres for Environmental Prediction (NCEP) and by the storm model. The latter (Jelesnianski, 1965) is expressed as follows:

$$\vec{W}_{sm}=\begin{cases}\dfrac{r}{R+r}\left(V_{ox}\vec{i}+V_{oy}\vec{j}\right)+W_R\dfrac{1}{r}\left(\dfrac{r}{R}\right)^{\frac{3}{2}}\left(A\vec{i}+B\vec{j}\right), 0<r\leqslant R,\\ \dfrac{R}{R+r}\left(V_{ox}\vec{i}+V_{oy}\vec{j}\right)+W_R\dfrac{1}{r}\left(\dfrac{R}{r}\right)^{\frac{1}{2}}\left(A\vec{i}+B\vec{j}\right), r>R,\end{cases} \tag{6}$$

where i and j are eastward and northward unit vectors, respectively; V_{ox} and V_{oy} are the components of moving velocity of the storm centre; r is the distance between the grid and storm centres; $\vec{W}_{sm}$ is the wind speed at radius r; and R is the radius of the maximum wind speed W_R.

$$A=-\left[\left(x-x_c\right)\sin\theta+\left(y-y_c\right)\cos\theta\right], \tag{7}$$

$$B=\left[\left(x-x_c\right)\cos\theta-\left(y-y_c\right)\sin\theta\right], \tag{8}$$

where (x, y) and (x_c, y_c) are the centre coordinates of the grid and storm, respectively; the inflow angle θ is taken as

$$\theta=\begin{cases}20^\circ, & r\leqslant R,\\ 15^\circ, & r>R.\end{cases} \tag{9}$$

We then overlaid this storm model onto the background wind field (NCEP) using a weight coefficient e and obtaining a synthetic wind field $\vec{W}_{\mathrm{sy}}$ (Wen et al., 2008):

$$\vec{W}_{\mathrm{sy}}=\vec{W}_{\mathrm{sm}}\left(1-e\right)+e\vec{W}_{\mathrm{ncep}}, \tag{10}$$

where $\vec{W}_{\mathrm{ncep}}$ is the NCEP wind field. The letter e is a weight coefficient determined as $e=\dfrac{\left(r/nR\right)^4}{1+\left(r/nR\right)^4}$ (n is usually taken to be 9 or 10). The coefficient e varies with the distance between the grid centre and storm centre. It ensures that the storm model is adopted in the vicinity of the tropical storm, but that the NCEP wind field is used away from the storm centre. Meanwhile, it also ensures a smooth transition between the two wind fields.

The pressure field for the tropical storm (Jelesnianski, 1965) is determined as follows:

$$P_a=\begin{cases}P_0+\dfrac{1}{4}\left(P_\infty-P_0\right)\left(\dfrac{r}{R}\right)^3, & r\leqslant R,\\ P_\infty-\dfrac{3}{4}\left(P_\infty-P_0\right)\left(\dfrac{R}{r}\right), & r>R,\end{cases} \tag{11}$$

where P_a is the sea surface pressure at r; P_0 is the pressure at the storm centre; and P_∞ is ambient pressure and is here assumed to be equal to 1020 hPa.

3. Numerical procedure

3.1 Model configuration

The coupled tide-surge model used in this study covered an area of the Bohai Sea, Yellow Sea, and East China Sea. The open boundaries were set along the first island chains and the Taiwan Strait. At this location, tides are provided by eight principal constituents (M2, S2, K1, O1, N2, K2, P1, Q1). The numerical model domain extends from 117.5°E to 131.5°E and from 24°N to 41°N; bathymetry data was obtained from E-TOP-5. The spherical grid has a resolution of 1/12th of a degree, that is, 5′×5′. The time step was set to 60 s.

The model was able to compute three water levels: the tide level without the effect of meteorological forcing (denoted by tidal model); a pure storm surge without regard to tidal impact (denoted by storm surge model); and total water level, considering tidal and meteorological forcing (denoted by coupled tide-surge model). In order to investigate the effects of tide-surge interactions on storm surge elevations, the model was run three times for each storm event (Zhang et al., 2007). During the first run, we calculated total water level with tidal and meteorological forcing. During the second run, we only simulated the tidal level using the tidal model. By subtracting the tidal level from the total water level, we obtained a storm surge elevation time series with the coupling effect of tide-surges. During the third run, we simulated the pure storm surge level using the storm surge model. When the pure storm surge elevation was subtracted from the storm surge elevation with coupling effects, we were able to obtain the water level caused by tide-surge interactions.

3.2 Case description

In the Bohai Sea, Yellow Sea, and East China Sea, the tide regularly rises and falls day after day. Typhoons occur, usually resulting from low-pressure systems, and can lead to a sharp rise or fall in seawater level, that is, storm surges. If these are combined with astronomical tides, abnormal increases or decreases in water level may occur, referred to as storm

tides (Kong, 2014). Specifically, flooding and ebbing tidal phases can affect the height and arrival time of peak surges (Sinha et al., 2008).

In this paper, we explore the influences of tide-surge interactions on storm surge elevations during Typhoon 7203 at several tidal stations. Figure 1 shows the track of Typhoon 7203 (from 25–28th July, 1972) and the locations of tidal stations. Typhoon data was available at six-hourly intervals.

A tide has steady high and low water elevations, but storm surge elevations are relevant to typhoon intensity and landing time. The interaction between tides and storm surges differs at different landing times. Different tide-surge interactions can thus cause differences in computational scenarios.

For the purpose of exploring the impacts of tide-surge interactions on storm surge elevations, we assumed that Typhoon 7203 arrived at 12 different times, with all other conditions remaining constant; that is, there were 12 independent cases for analysis. Specific processes were determined as per the following steps. Suppose that the start time of the first numerical experiment (hereafter, E1) was 08∶00 AM on 25th July, 1972; that is, the typhoon arrived at this time. In the second numerical experiment (hereafter, E2), the start time was 10∶00 AM on 25th July, 1972. The arrival time of the typhoon in E2 was two hours later than in E1. In other words, there was a two-hour lag between the two contiguous experiments; in this way, 12 cases were simulated. For all cases, background wind fields were taken from NCEP reanalysis surface winds data, spanning the period from 08∶00 AM on 25th July to 08∶00 AM on 28th July, 1972. Typhoon and pressure data were from Typhoon 7203. Each experiment lasted 72 h and was consistent with the time length of Typhoon 7203. In addition, 12 tidal levels were also simulated using the tidal model.

4. Results and discussion

4.1 Tides

When the tidal potential and open boundary terms are removed from eqs. (2), (3) and (5), the coupled tide-surge model is reduced to the storm surge model of Fan et al. (2011). The latter authors conducted verification of computed water surface elevation representing the Typhoon 7203-induced storm surge, based on field data at different tidal stations; model results showed that the numerical simulations of the storm surge were reasonable.

When the pressure term and wind stress term are removed from eqs. (2) and (3), the coupled tide-surge model is reduced to the tidal model of Lu et al. (2006). In the tidal

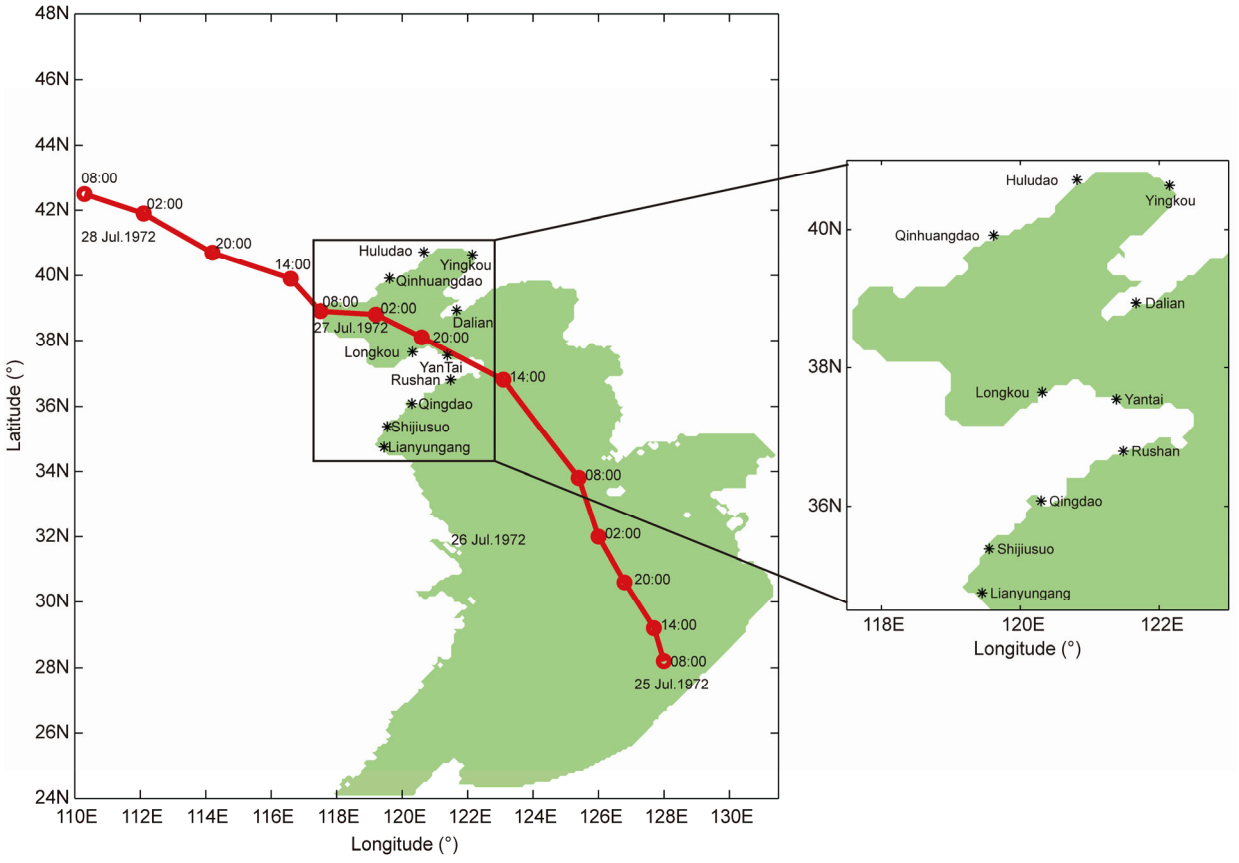

Figure 1 Asterisks denote tidal stations, solid lines represent the track of Typhoon 7203, and red circles indicate the typhoon time series.

model, the computing area, spherical resolution, and time step are the same as those of the coupled tide-surge model. Initial values of sea surface elevation and horizontal velocities were set to zero. The tidal model is driven by tidal potential and open boundary conditions. Tidal potential was calculated as per Fang et al. (1999), and the sea surface elevation on the open boundary condition was provided by eq. (5). The model start point was 27th April, 1972 and it ran for 90 days, with the possibility of harmonic analysis calculations for simulated results over the latter 60 days of the simulation. Table 1 lists absolute mean differences in amplitude and phase-lag of sea surface elevation between simulated results and observations at the 489 points of TOPEX/ Poseidon (T/P) tracks (as shown in Figure 2) for the four principal constituents M2, S2, K1, and O1. Their cotidal charts are shown in Figure 3, respectively.

4.2 Simulation and analysis of 12 storm surge elevations

By running the coupled tide-surge model, total water levels for each of the 12 cases were simulated. Similarly, astronomical tide levels were also calculated using the tidal model. Subtracting tide levels from total water levels allowed us to obtain a storm surge elevation time series with tide-surge coupling effects. Table 2 lists extreme values of the 12 storm surge elevations at 10 tidal stations during Typhoon 7203. Table 3 lists the maximum differences between the 12 extreme values for each tidal station.

As can be seen from Table 3, the maximum difference between the 12 extreme storm surge elevation values, of up

Table 1 Absolute mean differences in amplitude and phase-lag of sea surface elevation between simulated results and observations at T/P points for the four principal constituents M2, S2, K1, and O1

Tides	Amplitude (cm)	Phase-lag
M2	3.2	4.6°
S2	3.3	4.0°
K1	3.7	4.5°
O1	3.6	4.4°

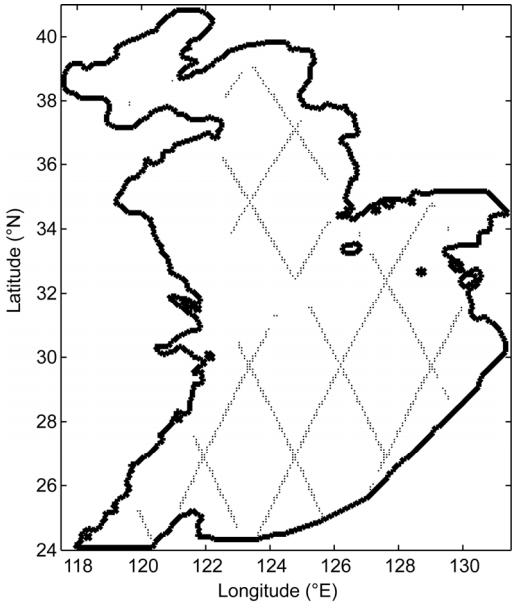

Figure 2 Dots denote the position of T/P observation points.

Table 2 Extreme values (cm) of 12 storm surge elevations at 10 tidal stations during Typhoon 7203 [a)]

Exp	Tidal stations									
	DL	YK	HLD	QHD	LK	YT	RS	QD	SJS	LYG
E1	101	168	158	163	119	130	−91	−97	−123	−147
E2	103	158	161	156	115	126	−94	−98	−125	−149
E3	101	139	154	142	116	131	−82	−93	−115	−127
E4	101	121	135	148	118	130	−78	−90	−110	−120
E5	94	117	122	150	109	129	−80	−92	−124	−147
E6	93	133	133	146	114	125	−84	−104	−128	−152
E7	97	162	148	145	115	123	−87	−96	−122	−145
E8	105	175	161	159	114	126	−93	−98	−118	−130
E9	103	171	170	162	119	132	−83	−87	−104	−111
E10	100	155	170	150	118	130	−73	−87	−103	−113
E11	103	137	150	161	109	127	−77	−95	−124	−143
E12	99	145	142	170	109	128	−79	−107	−128	−151

a) Acronyms DL, YK, HLD, QHD, LK, YT, RS, QD, SJS, and LYG refer to the 10 tidal station (Dalian, Yingkou, Huludao, Qinhuangdao, Longkou, Yantai, Rushan, Qingdao, Shijiusuo, and Lianyungang).

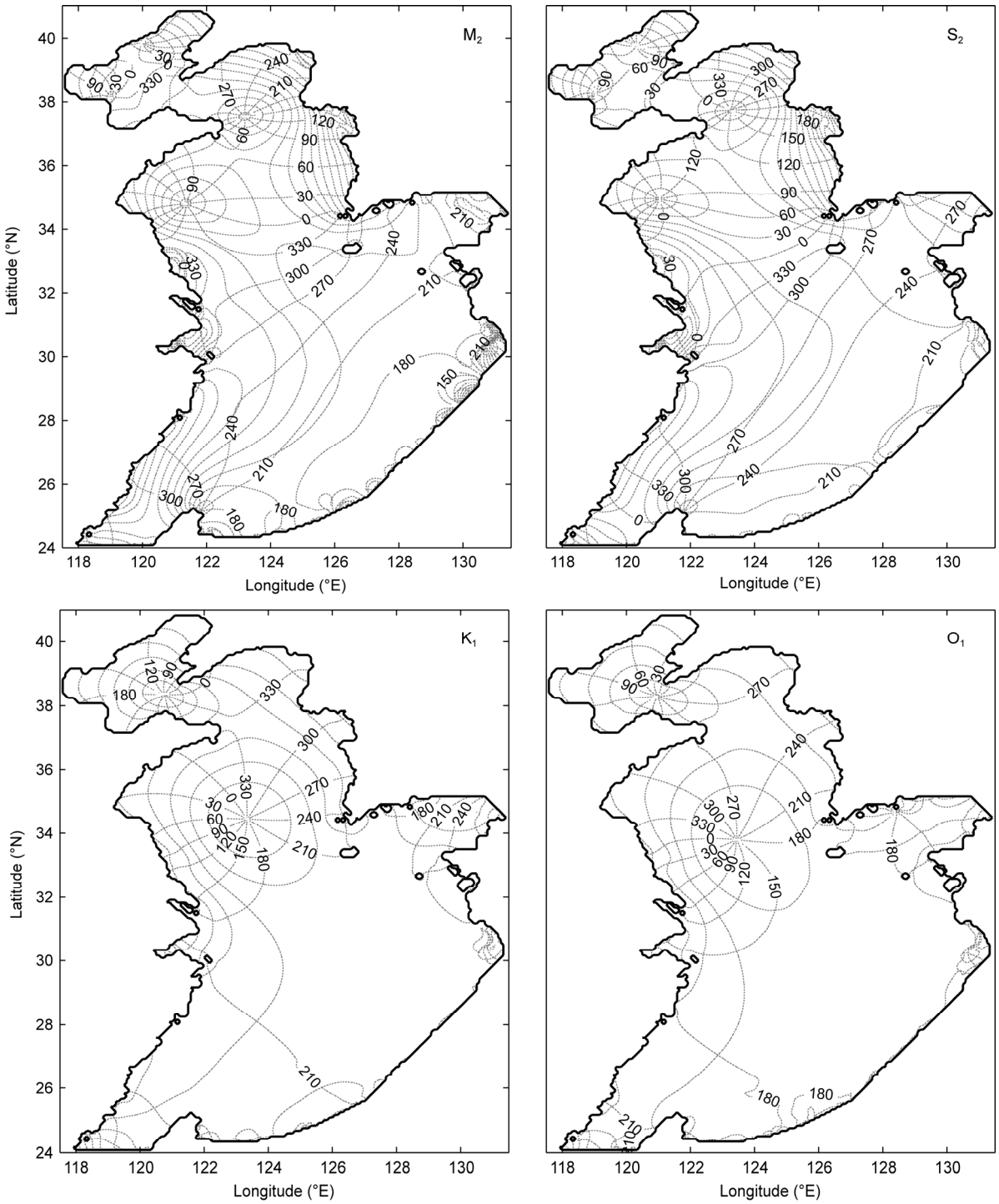

Figure 3 Model-produced cotidal charts for M2, S2, K1 and O1 constituents. Phase-lag (in deg); amplitude (in m) in [0.1, 3.0] m, with an interval of 0.2 m for the M2 constituent, 0.1 m for S2 constituent and 0.05 m for K1 and O1 constituents.

to 58 cm, was observed at Yingkou tidal station. Maximum differences for rising water were largest at Yingkou and Huludao, and at Shijiusuo and Lianyungang for falling water. Figure 4 shows extreme values of the 12 storm surge elevations at these four selected tidal stations, based on numerical simulation results.

In order to better understand the influences of tide-surge interactions on storm surge elevations, Figure 5 shows storm surge elevations with tide-surge coupling effects at four selected tidal stations. It can be noted that interactions between astronomical tides and storm surges at different landing times can lead to differences in storm surge elevations. The differences between the 12 storm surge elevations at each tidal station are very apparent, demonstrating

Table 3 Maximum differences (cm) between 12 extreme values at 10 tidal stations during Typhoon 7203[a)]

Tidal stations	DL	YK	HLD	QHD	LK	YT	RS	QD	SJS	LYG
Maximum difference	12	58	48	28	10	9	21	20	25	41

a) Acronyms DL, YK, HLD, QHD, LK, YT, RS, QD, SJS, and LYG refer to the 10 tidal stations (DaLian, Yingkou, Huludao, Qinhuangdao, Longkou, Yantai, Rushan, Qingdao, Shijiusuo, and Lianyungang).

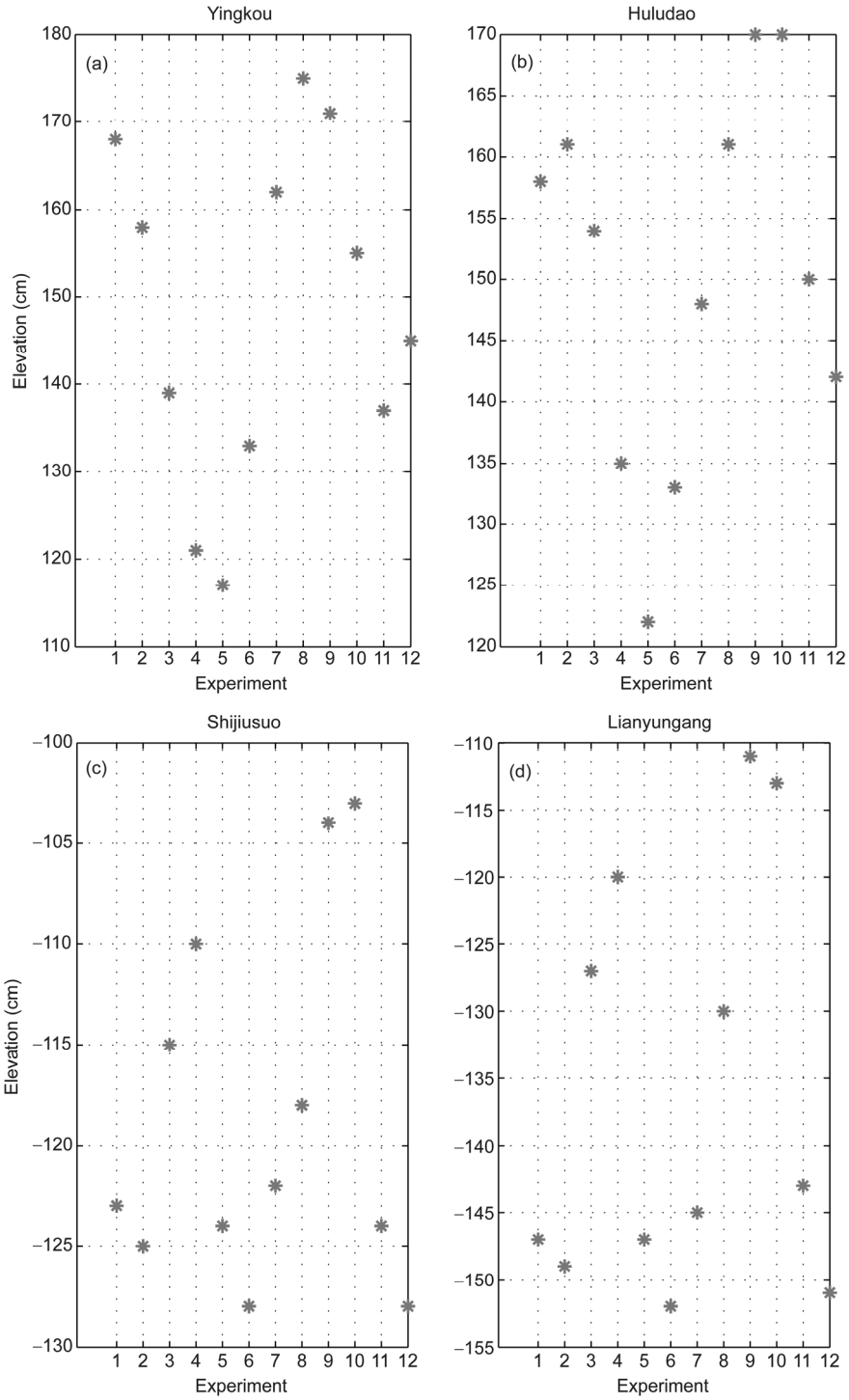

Figure 4 Extreme values (cm) of 12 storm surge elevations at Yingkou tidal station (a), Huludao tidal station (b), shijiusuo tidal station (c) and Lianyungang tidal station (d).

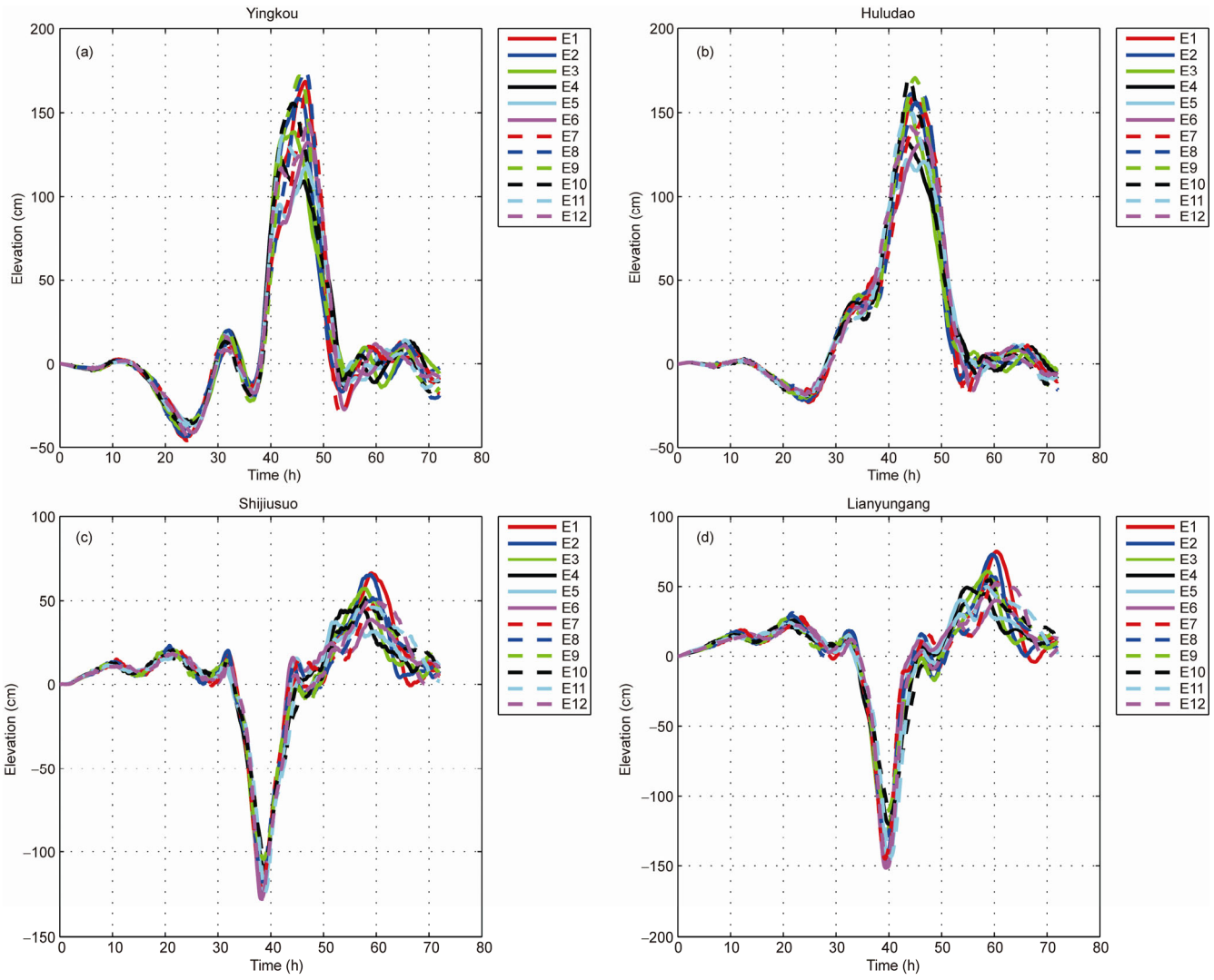

Figure 5 Storm surge elevations for the 12 cases at Yingkou tidal station (a), Huludao tidal station (b), shijiusuo tidal station (c) and Lianyungang tidal station (d).

the effects of tide-surge interactions, which must be considered in the prediction of storm surge elevations.

5. Conclusions

A coupled tide-surge model was developed in this study and applied to the Bohai Sea, Yellow Sea, and East China Sea. The model had a resolution of 1/12th of a degree. Storm surges and astronomical tides were simultaneously included in the numerical model. The tide was computed with open boundary conditions and tidal potential. Wind stress was provided by a synthetic wind field. Storm surge elevations, with coupled effects of tide-surge, were investigated in coastal regions.

To explore the effects of tide-surge interactions on storm surges, total water levels and tide levels for 12 cases were simulated, assuming that Typhoon 7203 arrived at 12 different times. The storm surge elevation, that is, the difference between total water level and tide level, was calculated for each tidal station. Numerical simulation results indicated that the maximum differences between the 12 extreme storm surge elevation values were 58 and 48 cm at YingKou and HuLuDao tidal stations, respectively. At ShiJiuSuo and LianYunGang tidal stations, the largest differences for falling water values were 25 and 41 cm, respectively. The impacts of tide-surge interactions must therefore be taken into account in prediction of storm surge elevations.

Acknowledgements *This research was provided by the National Natural Science Foundation of China (Grant No. 41371496), the National Science and Technology Support Program (Grant No. 2013BAK05B04), the Natural Science Foundation of Shandong Province of China (Grant No. ZR2014DM017), the Opening Fund of Shandong Provincial Key Laboratory of Marine Ecology and Environment & Disaster Prevention and Mitigation (Grant No. 201411), and the Applied Research Fund for Postdoctoral Researchers of Qingdao (Grant No. 82214263).*

References

Antony C, Unnikrishnan A S. 2013. Observed characteristics of tide-surge interaction along the east coast of India and the head of Bay of Bengal. Estuar Coast Shelf Sci, 131: 6–11

Chen W B, Liu W C, Hsu M H. 2012. Predicting typhoon-induced storm surge tide with a two-dimensional hydrodynamic model and artificial neural network model. Nat Hazards Earth Syst Sci, 12: 3799–3809

Fan L L, Liu M M, Chen H B, Lv X Q. 2011. Numerical study on the spatially varying drag coefficient in simulation of storm surges employing the adjoint method. Chin J Oceanol Limnol, 29: 702–717

Fang G H, Kwok Y K, Yu K J, Zhu Y H. 1999. Numerical simulation of principal tidal constituents in the South China Sea, Gulf of Tonkin and Gulf of Thailand. Cont Shelf Res, 19: 845–869

Haigh I D, Wijeratne E M S, MacPherson L R, Pattiaratchi C B, Mason M S, Crompton R P, George S. 2014. Estimating present day extreme water level exceedance probabilities around the coastline of Australia: Tides, extra-tropical storm surges and mean sea level. Clim Dynam, 42: 121–138

Jelesnianski C P. 1965. A numerical calculation of storm tides induced by a tropical storm impinging on a continental shelf. Mon Weather Rev, 93: 343–358

Kong X P. 2014. A numerical study on the impact of tidal waves on the storm surge in the north of Liaodong Bay. Acta Oceanol Sin, 33: 35–41

Li Y N, Peng S Q, Yan J, Xie L. 2013. On improving storm surge forecasting using an adjoint optimal technique. Ocean Model, 72: 185–197

Lin N, Emanuel K, Oppenheimer M, Vanmarcke E. 2012. Physically based assessment of hurricane surge threat under climate change. Nat Clim Change, 2: 462–467

Lu X Q, Zhang J C. 2006. Numerical study on spatially varying bottom friction coefficient of a 2D tidal model with adjoint method. Cont Shelf Res, 26: 1905–1923

Maspataud A, Ruz M, Vanhee S. 2013. Potential impacts of extreme storm surges on a low-lying densely populated coastline: the case of Dunkirk area, Northern France. Nat Hazards, 66: 1327–1343

Olbert A I, Nash S, Cunnane C, Hartnett M. 2013. Tide-surge interactions and their effects on total sea levels in Irish coastal waters. Ocean Dynam, 63: 599–614

Park Y H, Suh K D. 2012. Variations of storm surge caused by shallow water depths and extreme tidal ranges. Ocean Eng, 55: 44–51

Peng S Q, Xie L. 2006. Effect of determining initial conditions by four-dimensional variational data assimilation on storm surge forecasting. Ocean Model, 14: 1–18

Peng S Q, Xie L, Pietrafesa L J. 2007. Correcting the errors in the initial conditions and wind stress in storm surge simulation using an adjoint optimal technique. Ocean Model, 18: 175–193

Pousa J L, D'Onofrio E E, Fiore M M E, Kruse E E. 2013. Environmental impacts and simultaneity of positive and negative storm surges on the coast of the Province of Buenos Aires, Argentina. Environ Earth Sci, 68: 2325–2335

Tang J, Shi J, Li X Q, Deng B, Jin M M. 2013. Numerical simulation of typhoon waves with typhoon wind model (in Chinese). Trans Oceanol Limnol, 2: 24–30

Sinha P C, Jain I, Bhardwaj N, Rao A D, Dube S K. 2008. Numerical modeling of tide-surge interaction along Orissa coast of India. Nat Hazards, 45: 413–427

Wen B, Wang P, Wan L, Zhang F R. 2008. Experiments on the simulation of typhoon waves in the inshore area of China Sea (in Chinese). Marine Sci Bull, 27: 1–6

Wu J. 1982. Wind-stress coefficients over sea surface from breeze to hurricane. J Geophys Res, 87: 9704–9706

Yang G B, Lu L G, Yuan Y L, Jiang Y, Liu Z W, Yang C M, Liu H M, Chen Z. 2015. Observations and analysis of environment and acoustic field changed by the passage of typhoon Damrey in the Yellow Sea in 2012. Sci China Earth Sci, 58: 2260-2270

Yang Z Q, Wang T P, Leung R, Hibbard K, Janetos T, Kraucunas I, Rice J, Preston B, Wilbanks T. 2014. A modeling study of coastal inundation induced by storm surge, sea-level rise, and subsidence in the Gulf of Mexico. Nat Hazards, 71: 1771–1794

Yin B S, Xu Z H, Huang Y, Lin X. 2009. Simulating a typhoon storm surge in the East Sea of China using a coupled model. Prog Nat Sci, 19: 65–71

You S H, Seo J W. 2009. Storm surge prediction using an artificial neural network model and cluster analysis. Nat Hazards, 51: 97–114

Zhang S W, Xie L L, Zhao H, Hou Y J. 2014. Tropical storm-forced near-inertial energy dissipation in the southeast continental shelf region of Hainan Island. Sci China Earth Sci, 57: 1879-1884

Zhang W Z, Hong H S, Shang S P, Chen D W, Chai F. 2007. A two-way nested coupled tide-surge model for the Taiwan Strait. Cont Shelf Res, 27: 1548–1567